Research Article Vol. 1, No. 9 / 15 Oct 2022 / *Optics Continuum* 1896

OPTICS CONTINUUM

Creation of a high-resolution atomic frequency comb and optimization of the pulse sequence for high-efficiency quantum memory in $^{167}Er:Y_2SiO_5$

S. YASUI,[1,2] M. HIRAISHI,[1,3] A. ISHIZAWA,[1] H. OMI,[4] T. INABA,[1] X. XU,[1] R. KAJI,[2] S. ADACHI,[2] AND T. TAWARA[5,*]

[1]*NTT Basic Research Laboratories, NTT Corporation, Atsugi, Kanagawa 243-0198, Japan*
[2]*Graduate School of Engineering, Hokkaido University, Sapporo, Hokkaido 060-8628, Japan*
[3]*The Dodd-Walls Centre for Photonic and Quantum Technologies, Department of Physics, University of Otago, Dunedin 9016, New Zealand*
[4]*Faculty of Science and Engineering, Yamato University, Suita, Osaka 564-0082, Japan*
[5]*College of Engineering, Nihon University, Koriyama, Fukushima 963-8642, Japan*
[*]*tawara.takehiko@nihon-u.ac.jp*

Abstract: We created high-resolution atomic frequency combs (AFCs) and optimized the pulse sequence used in AFC memory to realize highly efficient AFC quantum memory using the $^{167}Er^{3+}:Y_2SiO_5$ hyperfine level system. As a result, the formation and relaxation times of AFCs were revealed, and AFCs with a resolution of 800 kHz were created by using an appropriate pump light intensity. An efficiency of 0.16% with a memory time of 0.5 µs was achieved even under a zero magnetic field and a 10 ppm Er concentration sample. This result paves the way for realizing highly efficient communication-wavelength AFC quantum memory.

1. Introduction

The key to developing quantum repeaters, which are indispensable for realizing global quantum information networks, is the rapid development of quantum memories (QMs) [1–3]. Rare-earth ion-doped crystals are promising QM materials because they are solid-state materials with good optical properties, and they are being actively studied [4–6]. Among them, $Er^{3+}:Y_2SiO_5$ (YSO) has optical transitions within the communication wavelength band. The advantage of this transition enables photon storage without wavelength conversion, which can be a bottleneck for efficiency. In addition, $^{167}Er^{3+}$:YSO crystals, which consists only of $^{167}Er^{3+}$ with a non-zero nuclear spin of $I = 7/2$ and hyperfine (HF) structure due to isotope purification, has a much longer optical coherence time of $T_2^{\text{opt}} \sim 10\ \mu$s and HF coherence time of $T_2^{\text{hyp}} \sim 370\ \mu$s under a zero magnetic field [7,8]. Moreover, erbium electron spin relaxation due to the magnetic fluctuation of yttrium ions via superhyperfine (SHF) interaction is suppressed by applying a high magnetic field. As a result, coherence is improved by the frozen core effect, and homogeneous linewidths of $\Gamma_h = 73$ Hz [9], $T_2^{\text{opt}} \sim 1.3$ ms [10], and $T_2^{\text{hyp}} \sim 1.3$ s have been obtained under a magnetic field of 7 T [11]. Furthermore, QM protocols such as the electromagnetically induced transparency [12], noiseless photon-echo [13], controlled reversible inhomogeneous broadening/gradient echo memory [14–16], revival of silenced echo [17], and atomic frequency combs (AFCs) [18,19] have been well studied on rare-earth doped materials. Among them, AFC QM protocols have been actively studied, such as 1-hour AFC memory with $^{151}Eu^{3+}$:YSO with spin wave storage [20] and 22% efficiency with 0.66 µs of storage in 50 ppm of $^{167}Er^{3+}$:YSO under 7 T with proper initialization of populations [21].

The bottleneck in achieving efficient and long-memory-time AFC QM protocols is the creation of high-quality AFCs [21–23]. A superior AFC is characterized by a large comb finesse F,

#457429 https://doi.org/10.1364/OPTCON.457429
Journal © 2022 Received 1 Mar 2022; revised 5 Aug 2022; accepted 5 Aug 2022; published 17 Aug 2022

OPTICS CONTINUUM

which means high resolution, and a large absorption depth (AD), which indicates high contrast. These parameters, F and AD, determine the efficiency and memory time of an AFC, and they are greatly affected by the frequency fluctuations of the light source and the intrinsic homogeneous linewidth of the material. Compared with praseodymium and europium ions, $^{167}Er^{3+}$ has an electronic spin $S = 1/2$, and the coupling to the nuclear spins of host crystal results in a relatively large homogeneous linewidth of electrons. Therefore, AFC memory of light and single photons in $^{167}Er^{3+}$:YSO has not been reported under a zero magnetic field. As it is mentioned above, the SHF interaction has been reported to be suppressed by applying a magnetic field. However, the memory time and efficiency are still much smaller than those of Pr:YSO and Eu:YSO [21,22]. As a result, achieving a long memory time and high efficiency with $^{167}Er^{3+}$:YSO is currently very difficult, and the realization of QM in the communication wavelength band is a challenging task.

The most effective way to solve this problem is to suppress the homogeneous linewidth by applying a magnetic field, but considering the actual construction of multiple quantum repeater nodes, it is necessary to construct a system to apply a magnetic field to all nodes. In addition, if the $^{167}Er^{3+}$:YSO is to operate not only as a QM for entanglement swapping but also as a transducer between microwaves and light, it should be under a zero magnetic field [8,24]. Therefore, it is also important to eliminate other factors that degrade the quality of AFCs. For creation of AFCs, a burn-back method [21,25] and a pulse-train method [26,27] are mainly used. In both methods, optical pumping by spectral hole burning (SHB) is used. Hence, the loss in AFC resolution due to power broadening and the loss of stored photons due to background absorption (BA) are factors that degrade AFC quality. Here, BA represents the absorption not contributing to memory by AFC and is caused by incomplete optical pumping. In the pulse-train method to create AFCs, it leads to higher quality of AFCs that optimizing the pump light intensity to minimize the effect of power broadening while maintaining a sufficient AD. In addition, optimizing the pulse sequence in the memory protocol by revealing the AFC generation and relaxation time, i.e., the time evolution of AD and BA, also leads to improve the efficiency. For higher efficiency AFC QM, the optimization of the pulse-train shape [28,29] and initialization methods [21] for electron populations in complex HF sublevels have been proposed and reported in various systems to improve the preparation step of AFC. However, we believe that the detailed investigation of the effects of power broadening and pulse sequences on efficiency of AFC in this study is very useful for the production of high-quality AFC, and the findings will help many AFC QM studies because the obtained knowledge can be used in different rare-earth-doped crystals.

In this paper, we demonstrate high-resolution AFCs with an optimized pulse sequence using the $^{167}Er^{3+}$:Y_2SiO_5 HF level system. First, we explored the optimal optical pumping condition that combines a large AD (i.e., small BA) and minimized power broadening by stabilizing the frequency of the light source using a fiber laser comb. Following that, high-resolution AFCs were created using the pulse-train method with an optimized light intensity. The duration of the AFCs was determined using time-resolved (TR-)SHB, and the AFCs were used for optical pulse storage. To improve the memory efficiency and avoid the spontaneous emission noise, we optimized the pulse-train irradiation time and the interval until the photon to be stored is injected. As a result, the efficiency was improved to 0.16% with a memory time of 0.5 µs, and by optimizing the AD, an efficiency of more than 20% can be expected even under a zero magnetic field. Therefore, the results reported in this paper indicate that high-efficiency and long-memory-time AFC QM can be realized by selecting the appropriate pump intensity and optimizing the sequence.

2. Creating atomic frequency comb

The memory efficiency of AFC-based QM protocols is determined by the quality of the created AFC. The important parameters are the comb finesse, $F = \Delta/\gamma$ (Δ : comb spacing, γ : comb width), AD, and BA. M. Afzelius *et al.* reported that when AD is sufficiently large, a memory efficiency of up to 54% can in principle be achieved with forward propagation by realizing

OPTICS CONTINUUM

$d/F = 2$ (d : AD) [18]. Since the memory time of light by AFC is $t = 1/\Delta$, it is essential to create a high-quality AFC with a high resolution and high contrast. It indicates a large AD with a small comb tooth width γ, for long time storage while maintaining an appropriate F. Since AFCs are created by frequency-selective optical pumping based on SHB with an inhomogeneously broadened absorption spectrum, γ depends on the width of the hole spectrum. This is determined by the homogeneous linewidth on optical transitions, the power broadening effect, and the frequency fluctuation of the light source, which must be suppressed to obtain high-resolution AFCs. To obtain a high-contrast AFC with a large AD, it is necessary to increase the pump light intensity. In contrast, an appropriate intensity must be selected to avoid the power broadening effect when the intensity is increased. Specifically for the pulse-train method, the resolution of the AFC depends on the intensity of the pump light, and the AD is greatly reduced when Δ is small.

2.1. Sample and experimental setup

Figure 1 shows the measurement system used in this study. In this measurement system, the external cavity laser diode (ECLD: RIO, Grande) was highly frequency stabilized using a 100 MHz repetition rate fiber laser comb, as described in detail in Ref. 30. For the AFC spectrum, TR-SHB, and AFC echo measurements that are described in the next section, the first-order optical sideband of the frequency generated by electro-optic modulators (EOMs: iXblue, MX-LN) were used. The other sideband components were removed by band-pass filters (BPF: Yenista, XTM-50). In these measurements, a pulse train for AFC, pump/probe pulses for TR-SHB measurement, and input pulse for AFC echo measurement were created by pulse shaping using acousto-optic modulators (AOMs: Gooch & Housego, Fibre-Q). To obtain a large extinction ratio, two AOMs were used in each path. The sample was an isotopically purified $^{167}Er^{3+}$:YSO bulk crystal ($^{167}Er^{3+}$ purity: 96%, concentration: 10 ppm) cooled to 1.6 K in a zero magnetic field [30,31], and the optical pump light and probe/input pulse were irradiated along the b-axis of the sample in a counter-propagating arrangement. The spot diameter was 40 μm. A digital oscilloscope (Textronix, MSO64) was used to acquire the spectra, and superconducting nanowire single photon detector (SNSPD, Single Quantum, 78% quantum efficiency) was used to observe the AFC echoes. The AOM was inserted just before the detector to prevent the strong reflected pump light from reaching the SNSPD. Figure 1(b) shows the HF levels of $^{167}Er^{3+}$:YSO. Here, $|m_s\rangle$ and $|m_I\rangle$ denote the quantum numbers of electron and nuclear spins. The HF levels included in the transition between the Site 1 Stark levels of $^4I_{15/2}$ (Z_1)-$^4I_{13/2}$ (Y_1) were used in these measurements. To obtain a large AD, the frequency of the optical pumping was set to the center frequency of the inhomogeneous broadening (195.116706 THz). In order to maximize the absorption depth of the inhomogeneous broadening, we used linearly polarized light parallel to the D_2 direction for both the pump and probe beams. Optical transitions with relatively large dipole moments [10] $|m_I, m_s\rangle = |-7/2, \pm 1/2\rangle_g \rightarrow |-7/2, \pm 1/2\rangle_e$ can occur, and the electron populations in $|-7/2, \pm 1/2\rangle_g$ can be pumped to the other levels. The subscripts g and e represent the HF sublevels of the ground and excited levels, respectively. In fact, other $\Delta m_I = 0, \pm 1$ optical transitions can also occur, but we ignore them here because of their small branching ratios.

2.2. Properties of hole spectrum

We investigated the physical properties of the hole spectra formed by CW optical pumping for the preparation of high-quality AFCs. Figure 2(a) shows the hole spectrum formed in the inhomogeneous broadening of the $^4I_{15/2}$ (Z_1)-$^4I_{13/2}$ (Y_1) optical transition. The pump power was set to 1100 nW to obtain a large AD, and the probe power was set to 2 nW. The homogeneous width Γ_h of this sample was 179 kHz [30], but the observed hole width Γ_{hole} was broadened due to the power broadening effect. The relation between Γ_{hole} and pump intensity, described in Ref.

OPTICS CONTINUUM

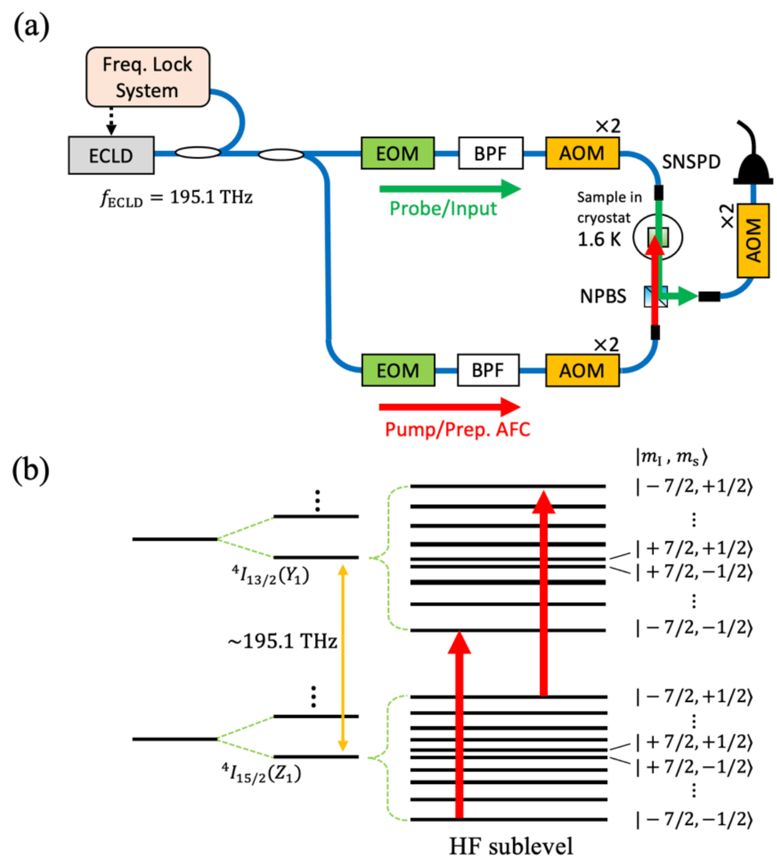

Fig. 1. (a) Measurement system. (b) Hyperfine level system of $^{167}Er^{3+}$:YSO. Red arrows indicate the transitions by optical pumping.

33, is as follows:

$$\Gamma_{\rm hole} = \sqrt{2}\Gamma_{\rm h}\sqrt{1+\sqrt{1+T_1^{\rm opt}T_2^{\rm opt}\Omega^2}} = \begin{cases} 2\Gamma_{\rm h} & (T_1^{\rm opt}T_2^{\rm opt}\Omega^2 \ll 1) \\ \sqrt{2}\Gamma_{\rm h}(T_1^{\rm opt}T_2^{\rm opt}\Omega^2)^{1/4} & (T_1^{\rm opt}T_2^{\rm opt}\Omega^2 \gg 1) \end{cases} \tag{1}$$

where $T_1^{\rm opt}T_2^{\rm opt}\Omega^2$ is the dimensionless intensity, $T_1^{\rm opt}$ is the optical population lifetime, $T_2^{\rm opt}$ is the optical coherence time, and Ω is the Rabi frequency. The above equation includes the effect of absorption during propagation in a sample of finite thickness, and it shows the limit when the absorption is large. Figure 2(c) shows the dependence of the hole width (FWHM) and hole saturation on the pump intensity, respectively. The hole width is well fitted by Eq. (1). Since the AD is small for low concentration samples, the AFC memory efficiency is mainly limited by the AD. Therefore, to achieve a large AD (small BA), which is a requirement for high-contrast AFCs, the hole spectrum needs to be saturated. However, as the pump light intensity increases, the hole width gets broadened due to the power broadening, and the resolution of AFCs decreases. Because of this trade-off, it is necessary to maintain the saturation condition while the intensity of pump light must be kept low as possible. For this reason, we set the pump light intensity to 1100 nW. We estimated the appropriate pump light intensity and created AFC with a high resolution of ~800 kHz while maintaining a large saturation (~88%).

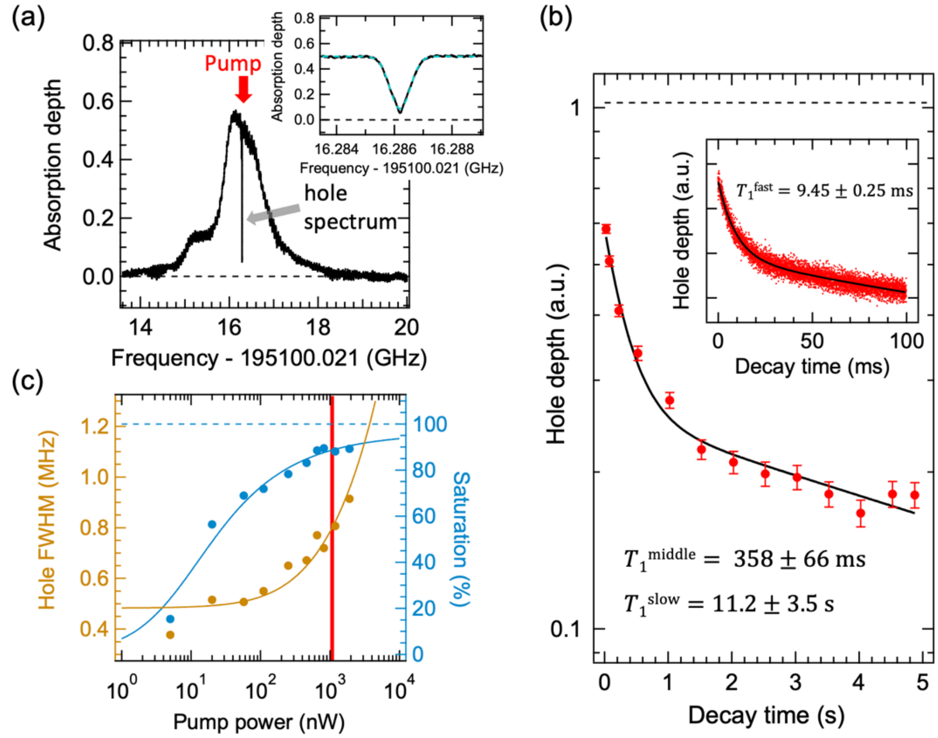

Fig. 2. (a) Inhomogeneous broadening of $^4I_{15/2}$ (Z_1)-$^4I_{13/2}$ (Y_1) optical transition and hole spectrum. Inset: magnified view of hole spectrum. Light blue dotted line is a Gaussian fitting. (b) TR-SHB measurement results. The vertical axis is a log scale. Black solid line is a double exponential fitting. Black dotted horizontal line represents zero-absorption level. Inset: Fast relaxation component. (c) Dependence of hole width (left axis) and hole saturation (right axis) on pump intensity. The solid yellow line is the fitting curve by Eq.(1). The solid light blue line is the fitting result from the analytical solution representing the saturation of the hole spectrum against the pump light intensity described in Ref. 32. Dotted light blue (yellow) horizontal line represents 100% saturation ($2\Gamma_h$). Red solid line is the pump light intensity used in this measurement.

Next, we investigated the dynamics of the hole spectrum, which is related to the duration of the AFC, by means of TR-SHB spectroscopy. First, the pump light was irradiated into the sample with a time width set to 50 ms. After a delay time, the probe light frequency was swept within the ±4-MHz band around the peak of the hole spectrum. The sweep time was set to 30 ms. The peak intensity of the hole spectrum was plotted at each delay time, and the decay of the spectral peak is shown in Fig. 2(b). The fast relaxation component [inset in (b)] was obtained by monitoring the variation in the transmitted light intensity of the probe light using SNSPD. These results indicate the existence of components with relaxation times of $T_1^{\mathrm{fast}} = 9.45 \pm 0.25$ ms, $T_1^{\mathrm{middle}} = 358 \pm 66$ ms, and $T_1^{\mathrm{slow}} = 11.2 \pm 3.5$ s, respectively. The relaxation component of T_1^{fast} corresponds to the decay from the optically excited level since the optical population lifetime reported by T. Böttger *et al.* has a similar value, $T_1^{\mathrm{opt}} \sim 10$ ms [34].

Here, we consider the origin of T_1^{middle} and T_1^{slow}. First, these relatively long lifetimes can be attributed to the transitions within the HF sublevels within $I_{15/2}$ (Z_1). Also, relaxation mechanisms in rare-earth ion-doped crystals consist of the spin-lattice relaxation (SLR) and the spin flip-flop mechanism. Under 1.6 K condition, the peak of the phonon density from the Boltzmann distribution is ~60 GHz, while the frequency range of the HF sublevels is ~10 GHz, which is relatively smaller than the former. Therefore, the contribution of SLR is small, and spin flip-flop is expected to be dominant. This relaxation mechanism was reported in isotopically purified $^{145}Nd^{3+}$:YSO crystals, which is Kramers ion with the same nuclear spin $I = 7/2$ as that of $^{167}Er^{3+}$:YSO [35]. In the reported model, the relaxing populations from the optically excited levels return to the pre-excited $|m_I, m_s\rangle$ level via either $\Delta m_s = \pm 1,\ \Delta m_I = 0$ path (transition A) or $\Delta m_s = \pm 1,\ \Delta m_I = \pm 1$ path (transition B). Here, the transition A represents electron-only spin-flip relaxation and the transition B represents electron and nuclear spin-flip relaxation. Transition B has a longer relaxation time than transition A because it also requires a nuclear spin flip [36]. In addition, a relaxation with $\Delta m_s = 0$ (transition C) can also occur, however, in this case, the relaxation time is determined only by the contribution of the SLR since it does not involve electron spin flip-flop. In Ref. 11, this relaxation time is reported to be 60 s, which is much larger than T_1^{slow}. Furthermore, the contribution of SLR is very small, and thus transition C can be neglected. In Ref. 35, they reported that the relaxation times of transitions A and B are 75 ms and 1.72 s, respectively, depending on the irradiation time of the pump light. Although the relaxation times are different between $^{145}Nd^{3+}$:YSO and $^{167}Er^{3+}$:YSO due to the different parameters such as the HF sublevels spacings and the optical transition wavelength, our results are qualitatively consistent in that they have two relaxation components, one on the order of milliseconds and the other on the order of seconds. In addition, the relaxation time of the electron spin flip-flop in non-purified Er^{3+}:YSO without nuclear spins under weak magnetic field is 129 ms [37], which corresponds to Transition A and is the same order of magnitude as T_1^{middle}. From these reasons, we assigned that T_1^{middle} and T_1^{slow} are the relaxation times corresponding to transition A and transition B, respectively, which are referred to as T_1^{hyp} in other reports. Further studies are needed to establish a clear origin and relaxation mechanisms of these hole lifetimes, which is a future challenge.

These T_1^{hyp} ‘s are much longer than the reported $^{167}Er^{3+}$:YSO (T_1^{hyp}= 97 ms [38]) at 50 ppm concentration. This is attributed to the fact that the Er concentration used in this study is 10 ppm, which greatly suppresses the spin flip-flop mechanism. Compared to Pr:YSO and Eu:YSO, $^{167}Er^{3+}$:YSO at 50 ppm has been difficult to create high-quality AFC under zero magnetic field due to the short T_1^{hyp}, which prevents sufficient preparation time of AFC and efficient optical pumping. The present observations show that a lower concentration of $^{167}Er^{3+}$ is very effective in improving the T_1^{hyp}.

Finally, when storing single photons in the AFC QM protocol, it is necessary to leave a time interval longer than the optical excitation lifetime between the creation of the AFC and the injection of the single photon to be stored. The reason for this is to avoid fidelity reduction due to spontaneous emission. Therefore, the results show that the BA increases by $\Delta d_0 = 0.05$ (d_0 : BA) when the time interval of 10 ms is used.

To summarize so far, we have estimated the appropriate pump intensity to produce high-quality AFCs, and the relaxation time of the hole spectrum, which corresponds to the relaxation time of the AFC, and the variation of BA, which increases as the AFC relaxes.

2.3. AFC quality

We used the pulse-train method to create an AFC by using a Gaussian pulse pair (Fig. 3). The pulse width was 100 ns, and the memory bandwidth was 10 MHz. The pulse spacings were 0.5 µs and 1 µs, and the AFC spectra were then acquired with comb spacings of $\Delta = 2$ MHz (red curve) and 1 MHz (blue curve), respectively. As a reference, the hole spectrum (black curve) was also depicted. The average power of the pulse train was 1100 nW, which is the optimal value and was estimated in the previous section. The BA of the AFC spectrum was increased compared to the hole spectrum. Since the energy splitting of the SHF sublevels is ~1 MHz [22,38], the generated anti-hole is included in the 10-MHz memory bandwidth of the pulse train. Therefore, the BA is expected to increase unfortunately because the anti-hole is also excited at the same time. Table 1 summarizes the parameters related to the quality of the AFC.

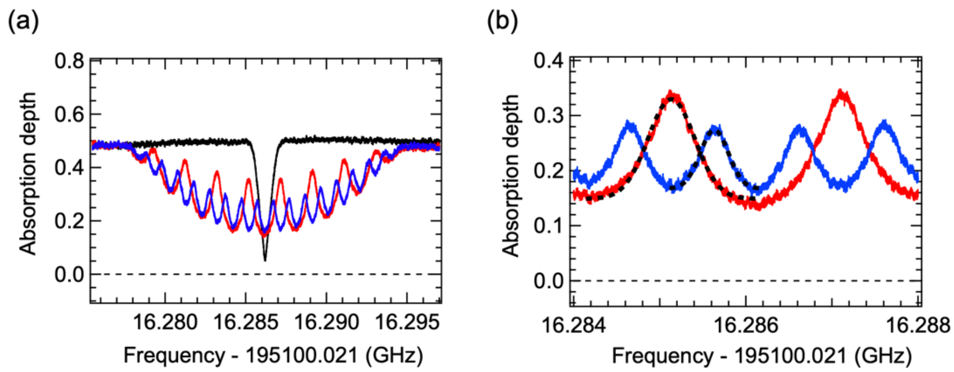

Fig. 3. (a) AFC produced by pulse-train method. Black: hole spectrum. Red: 2-MHz comb spacing. Blue: 1-MHz comb spacing. (b) Magnified view of AFC. Black dotted lines are Gaussian fittings.

Table 1. Important parameters of AFC

Δ	γ	F	d (AD)	d_0 (BA)
2 MHz	638 kHz	3.13	0.196	0.149
1 MHz	386 kHz	2.59	0.106	0.167

Table 1 shows that the AD and comb finesse F decreased as the comb spacing Δ decreased. This is due to the resolution, which is determined by the hole width. In other words, it is due to the spectral envelope of the pulse train being convoluted with the hole width of 800 kHz. The effect of this resolution on the efficiency of the AFC echo is discussed in the next section. Consequently, it is essential to suppress the hole width as much as possible to achieve a long memory time. There are several ways to get narrower hole width even under zero-magnetic fields. Firstly, further lowering the concentration of $^{167}Er^{3+}$ would be effective. This should result in narrower homogeneous linewidth owing to reduction of Er^{3+}-Er^{3+} interactions [31]. Although this also reduces AD to some extent, as we mention later in this section, low AD can be compensated with implementation optical resonators. Secondly, excluding nucleus in host materials by isotopic purifications. For instance, it is technically possible to purify Si by ^{28}Si; $Y_2{}^{28}SiO_5$. This reduces magnetic fluctuation of $^{167}Er^{3+}$ from the environment, leading to narrower homogeneous linewidths.

Since the effect of power broadening is proportional to the homogeneous linewidth from Eq. (1), the increase in the hole width due to power broadening can be suppressed by narrowing the homogeneous linewidth itself. For example, if the homogeneous linewidth is suppressed to 50 kHz, the hole width including power broadening becomes ~200 kHz, which enables the creation of higher quality of AFCs. The improved resolution of the AFC is also expected to increase the AD of the AFC up to the upper limit of the difference (d_{max} ~ 0.35 in this sample) between the AD of the inhomogeneous broadening (d_{inh} ~ 0.50) and BA (d_0 ~ 0.15). Because the present measurement uses a low Er concentration sample of 10 ppm, the absolute efficiency is severely limited by the small AD. The AD can be improved by introducing an appropriate population initialization process [39] or by fabricating an optical cavity to enhance the light-matter interaction [40,41].

3. Observation of AFC echo

Next, we observed AFC echoes by inputting stored light pulses with a pulse width of 100 ns and a peak intensity of 400 nW into the created AFC. Figure 4(a) shows the pulse sequence used for the measurements. The sequence was optimized to maximize the efficiency of the AFC echo generation as described below. The AFC was created by shaping the Gaussian pulse train within a time range of 10 µs and repeating it 2000 times. After an interval of 10 ms to avoid an increase in noise due to spontaneous emission, the stored input pulse was injected 2000 times, and the AFC echo was integrated. The memory efficiency was obtained by comparing the AFC echo with the reference light passing through the transparent (non-absorbing) region of $^{167}Er^{3+}$:YSO. The reference signal was obtained by decreasing the optical frequency of the input pulse by 4 GHz. Figure 4(b) shows the observed AFC echoes for the AFC with the comb spacings of Δ = 2 MHz (red) and 1 MHz (blue). The echo efficiencies were 0.16 ± 0.01% and 0.05 ± 0.01%, respectively, and the decrease in efficiency can be attributed to the decrease in the contrast of the AFC. The inset of Fig. 4(b) shows the efficiency of the AFC echo versus memory time. Here, we also plot the memory efficiency of AFCs created by varying the comb spacing Δ from 0.25 to 4 MHz. The efficiency at memory times of $1/\Delta = 0.25$ μs and 0.50 µs was almost unchanged, but the echo efficiency decreased exponentially at memory times after 0.50 µs. This can be attributed to the fact that the resolution of the AFC was 800 kHz, which caused a rapid decrease in the comb finesse and AD with the inverse (1.25 µs) as the threshold. Figure 4(c) shows the effect of the averaged power of the pulse train on the AFC echo intensity. The efficiency increased up to around 2000 nW and then decreased. Compared with Fig. 2(c), this increase

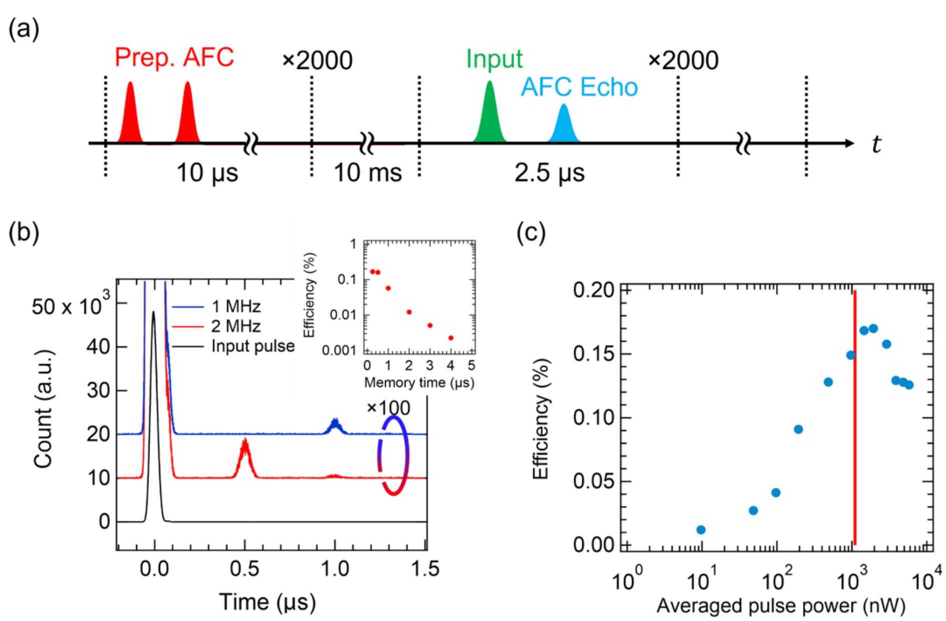

Fig. 4. (a) Sequence of pulse-train method. (b) Observed AFC echo; black solid line represents input pulse to be stored, red (blue) solid line represents that for Δ=2 MHz (1 MHz) AFC. AFC echo expands by factor of 100. Inset: memory efficiency vs. storage time. (c) AFC echo efficiency versus averaged pulse intensity of pulse train used to create AFC. Red line indicates the average pulse intensity used (1100 nW).

reflects that in AD associated with the formation of the AFC. The subsequent decrease was caused by the fact that the resolution of the AFC continued to decrease while the AD increased more slowly as shown in Fig. 2(c). In other words, the effect of the decrease in AD in resolution with increasing excitation intensity exceeds the effect of the increase in AD in AFC formation.

Furthermore, we optimized the pulse sequence to improve the efficiency of the AFC echo. Figure 5(a) shows the dependence of irradiation time of the pulse train to form AFC, which reflects the formation time of the AFC. It is suggested that the AD increases as the formation of the AFC, and thus, the echo efficiency increases. The figure shows that sufficient optical pumping can be obtained by irradiating for more than 20 ms, and we adopted this irradiation time as the optimal pump duration in this measurement. Figure 5(b) depicts the efficiency as a function of the interval duration between the creation of the AFC and the irradiation of the stored input pulse. This reflects the relaxation time of the AFC, which is in good agreement with the T_1^{fast} and T_1^{middle} decay constants of the AFC revealed by the TR-SHB results shown in Fig. 2(b). For the storage of single-photon-level optical pulses, an interval of $T_1^{\mathrm{opt}} = 10$ ms or more is required, although the AD is reduced to avoid noise due to spontaneous emission. Then, we set the interval to 10 ms to preserve the single photon level for future work. As a result, we obtained an echo efficiency of 0.16% with a memory time of 0.5 μs.

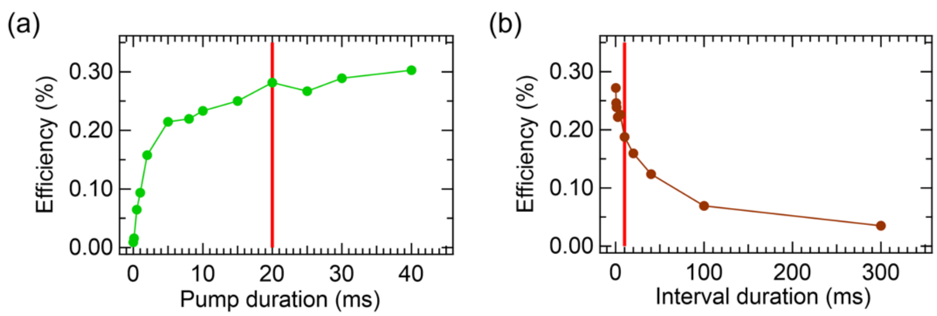

Fig. 5. Optimization of pulse sequences. (a) Echo efficiency versus irradiation time by pulse train. (b) Echo efficiency versus interval after AFC creation. Red vertical lines are the times used for echo measurement in Fig. 4(b). Memory time for measurement is 0.5 μs.

We performed the memory storage of optical pulses using a high-resolution AFC and clarified the echo decay. To further improve the echo efficiency, we optimized the pulse sequence. Furthermore, by varying the parameters of the pulse sequence for the echo efficiency, the formation time of the AFC was newly clarified, and the relaxation time was found to be in good agreement with the TR-SHB results.

4. Discussion

To evaluate the obtained memory efficiency for each memory time, we calculated the AD and F dependencies of the efficiency of the AFC echo, as reported in Ref. 18, considering the effect of BA described in Ref. 27. Here, the efficiency η can be expressed as follows, considering a Gaussian-shaped AFC for simplicity:

$$\eta \approx (d/F)^2 e^{-d/F} \cdot e^{-7/F^2} \cdot e^{-d_0}. \tag{2}$$

The first term is related to the absorbance of the photon according to Beer's law. The second term is the degradation in efficiency due to the decoherence that occurs between the times at which a photon is absorbed and is emitted as an echo. The third term represents the loss of photons due to BA during propagation through the material.

OPTICS CONTINUUM

The dependencies of the memory efficiency on the comb finesse and AD are shown in Fig. 6 with the parameters obtained in the measurement substituting into Eq. (2). Figure 6(a) shows that measured comb finesses close to the maximum efficiency were obtained. It originates from the fact that the resolution of 800 kHz is sufficient to obtain the comb finesses that maximizes the efficiency when the comb spacings were set to 2 MHz and 1 MHz. If the resolution is further reduced, the comb finesse decreases more when the comb spacing is reduced. Therefore, by setting the pump light intensity so that the resolution is as large as possible, the efficiency of the comb finesses was close to the maximum even at a comb spacing of 1 MHz. The experimental values are slightly larger than the calculated one. This can be attributed to the efficiency being very sensitive to the change in d. From Fig. 6(b), the current low memory efficiency was caused by the small AD. This was due to the low Er concentration of the current sample (10 ppm) and the short sample length (6 mm).

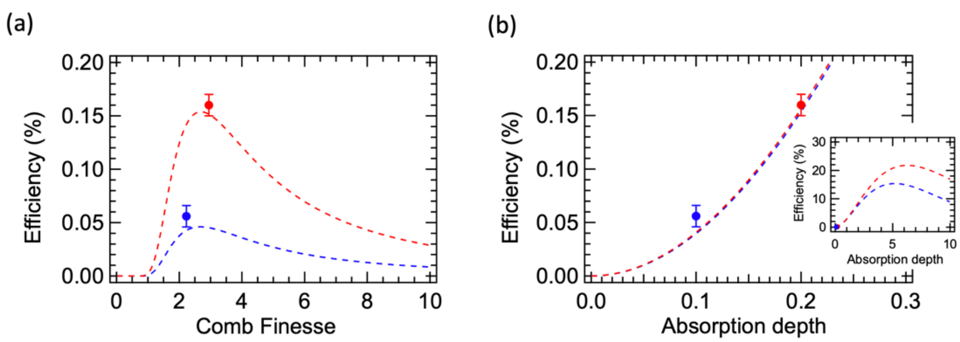

Fig. 6. Memory efficiency versus comb finesse (a) and AD (b) using Eq. (2). Blue and red markers represent efficiencies obtained from experiments with comb spacings of Δ = 1 MHz and 2 MHz, respectively. Dashed lines in each color are theoretical curves calculated from parameters in Table 1. Increase in BA due to decay of AFC (Δd_0 = 0.05) was considered. Inset: extended view of (b).

This material enables us to suppress Er^{3+}-Er^{3+} interactions, which are one of the sources of decoherence. In addition, the lower concentration improves T_1^{hyp} and extends AFC preparation time. Furthermore, the optical pumping efficiency is also improved, resulting in smaller BA under zero magnetic field [39]. For these reasons, we use a 10 ppm concentration of $^{167}Er^{3+}$:YSO instead of the 50 ppm concentration used in Refs. 21 and 22.

AFC QMs with efficiencies of 10~22% using $^{167}Er^{3+}$:YSO under the magnetic field have already been reported [21,42]. Achieving such a high efficiency under zero magnetic field is a challenging task. The current memory efficiency is very small (0.16%), but it was found that it can be improved to 12~22% by optimizing AD (d = 5~7). At this stage, we believe that it would be valuable and important to try to make a breakthrough to reach the theoretical limit of 54% under zero magnetic field. We are currently exploring ways, including stabilizing the optical frequency and reducing BA using appropriate initialization methods as shown in Ref. 39.

To realize practical QMs that can operate under zero magnetic field, it is essential to use materials with a narrow homogeneous linewidth, and therefore, low-concentration, high-purity $^{167}Er^{3+}$:YSO is a desirable platform. The current challenge is to improve the low memory efficiency, which, as shown above, is greatly limited by AD. However, this can be improved by introducing an appropriate population initialization process or by fabricating the optical cavity. Increasing the $^{167}Er^{3+}$ concentration and interaction length will improve AD, but will also increase BA. By using an initialization process, only AD can be increased without increasing BA. The optical transition frequencies of the HF sublevels overlap under zero magnetic field, and a proper initialization process under zero magnetic field is a challenge to overcome. In addition, if an optical cavity is used, AD can be increased by improving the light-matter interaction and T_1^{opt} can be reduced due to the Purcell effect. As a result, optical pumping efficiency is improved, and BA is reduced. By calculating the dependence of the memory efficiency on the AD, it was shown that an efficiency of 22% can be achieved at a memory time of 0.5 µs by optimizing the AD. To achieve an even higher efficiency and longer memory time, it is essential to achieve an even higher finesse by suppressing the homogeneous linewidth. For this purpose, it is essential to suppress the power broadening effect by optimizing the pump light intensity, as we have shown, as well as stabilizing the frequency of the light source. This is also the case when AFCs are created by the burn-back method using an anti-hole.

The present results are only a fixed delay line optical memory using AFC, and it is necessary to introduce spin-wave storage for on-demand readout and memory time extension. These have been well demonstrated in Eu:YSO and Pr:YSO, but require conversion and inverse conversion of optical coherence to nuclear spin coherence, which reduces memory efficiency. According to [43], these conversion efficiencies are approximately 60%, so if spin-wave storage is introduced with improved AD, the memory efficiency is expected to be 4∼8%.

5. Conclusion

We investigated the quality of AFCs from the view of their resolution and pulse sequences, which has a significant impact on the efficiency of AFC QM. As a result, we achieved frequency-selective optical pumping with a resolution of 800 kHz by using an appropriate pump light intensity to create a high-quality AFC using the $^{167}Er^{3+}:Y_2SiO_5$ hyperfine level system. In addition, by optimizing the pulse sequence used for memory, a 0.5-µs memory of optical pulses was achieved with an efficiency of 0.16%. Although the efficiency was low due to the low Er concentration, it was shown that a high memory efficiency of over 20% can be achieved even under a zero magnetic field by further improving the resolution by introducing an appropriate initialization process and improving the AD with the cavity-QED effect.

Funding. Japan Society for the Promotion of Science (19H02636, 21H01745, 22H01995).

Acknowledgments. We thank Dr. Ryuichi Ohta for the fruitful discussions.

Disclosures. The authors declare no conflicts of interest.

Data availability. Data underlying the results presented in this paper are not publicly available at this time but may be obtained from the authors upon reasonable request.

References

1. S. Wehner, D. Elkouss, and R. Hanson, "Quantum internet: A vision for the road ahead," Science **362**(6412), eaam9288 (2018).
2. M. K. Bhaskar, R. Riedinger, B. Machielse, D. S. Levonian, C. T. Nguyen, E. N. Knall, H. Park, D. Englund, M. Lončar, D. D. Sukachev, and M. D. Lukin, "Experimental demonstration of memory-enhanced quantum communication," Nature **580**(7801), 60–64 (2020).
3. H. J. Kimble, "The quantum internet," Nature **453**(7198), 1023–1030 (2008).
4. M. Zhong, M. P. Hedges, R. L. Ahlefeldt, J. G. Bartholomew, S. E. Beavan, S. M. Wittig, J. J. Longdell, and M. J. Sellars, "Optically addressable nuclear spins in a solid with a six-hour coherence time," Nature **517**(7533), 177–180 (2015).
5. G. Heinze, C. Hubrich, and T. Halfmann, "Coherence time extension in $Pr^{3+}:Y_2SiO_5$ by self-optimized magnetic fields and dynamical decoupling," Phys. Rev. A **89**(5), 053825 (2014).
6. R. M. Macfarlane, T. L. Harris, Y. Sun, R. L. Cone, and R. W. Equall, "Measurement of photon echoes in $Er:Y_2SiO_5$ at 1.5 µm with a diode laser and an amplifier," Opt. Lett. **22**(12), 871–873 (1997).
7. M. Hiraishi, M. IJspeert, T. Tawara, S. Adachi, R. Kaji, H. Omi, and H. Gotoh, "Optical coherent transients in $^{167}Er^{3+}$ at telecom-band wavelength," Opt. Lett. **44**(20), 4933–4936 (2019).
8. J. V. Rakonjac, Y.-H. Chen, S. P. Horvath, and J. J. Longdell, "Long spin coherence times in the ground state and in an optically excited state of $^{167}Er^{3+}:Y_2SiO_5$ at zero magnetic field," Phys. Rev. B **101**(18), 184430 (2020).
9. T. Böttger, C. W. Thiel, R. L. Cone, and Y. Sun, "Effects of magnetic field orientation on optical decoherence in $Er^{3+}:Y_2SiO_5$," Phys. Rev. B **79**(11), 115104 (2009).
10. M. Rančić, "High resolution spectroscopy of erbium doped solids," PhD thesis, the Australian National University (2018).

11. M. Rančić, M. P. Hedges, R. L. Ahlefeldt, and M. J. Sellars, "Coherence time of over a second in a telecom-compatible quantum memory storage material," Nat. Phys. **14**(1), 50–54 (2018).
12. M. Hain, M. Stabel, and T. Halfmann, "Few-photon storage on a second timescale by electromagnetically induced transparency in a doped solid," New J. Phys. **24**(2), 023012 (2022).
13. Y. -Z. Ma, M. Jin, D. -L. Chen, Z.-Q. Zhou, C. -F. Li, and G. -C. Guo, "Elimination of noise in optically rephased photon echoes," Nat. Commun. **12**(1), 4378 (2021).
14. B. Lauritzen, J. Minář, H. de Riedmatten, M. Afzelius, N. Sangouard, C. Simon, and N. Gisin, "Telecommunication-wavelength solid-state memory at the single photon level," Phys. Rev. Lett. **104**(8), 080502 (2010).
15. M. P. Hedges, J. J. Longdell, Y. Li, and M. J. Sellars, "Efficient quantum memory for light," Nature **465**(7301), 1052–1056 (2010).
16. B. Lauritzen, J. Minář, H. de Riedmatten, M. Afzelius, and N. Gisin, "Approaches for a quantum memory at telecommunication wavelengths," Phys. Rev. A **83**(1), 012318 (2011).
17. J. Dajczgewand, J.-L. Le Gouët, A. Louchet-Chauvet, and T. Chanelière, "Large efficiency at telecom wavelength for optical quantum memories," Opt. Lett. **39**(9), 2711–2714 (2014).
18. M. Afzelius, C. Simon, H. de Riedmatten, and N Gisin, "Multimode quantum memory based on atomic frequency combs," Phys. Rev. A **79**(5), 052329 (2009).
19. E. Saglamyurek, J. Jin, V. B. Verma, M. D. Shaw, F. Marsili, S. W. Nam, D. Oblak, and W. Tittel, "Quantum storage of entangled telecom-wavelength photons in an erbium-doped optical fibre," Nat. Photonics **9**(2), 83–87 (2015).
20. Y. Ma, Y. -Z. Ma, Z. -Q. Zhou, C. -F. Li, and G. -C. Guo, "One-hour coherent optical storage in an atomic frequency comb memory," Nat. Commun. **12**(1), 2381 (2021).
21. J. Stuart, M. Hedges, R. Ahlefeldt, and M. Sellars, "Initialization protocol for efficient quantum memories using resolved hyperfine structure," Phys. Rev. Res. **3**(3), L032054 (2021).
22. I. Craiciu, M. Lei, J. Rochman, J. M. Kindem, J. G. Bartholomew, E. Miyazono, T. Zhong, N. Sinclair, and A. Faraon, "Nanophotonic quantum storage at telecommunication wavelength," Phys. Rev. Appl. **12**(2), 024062 (2019).
23. M. Nicolle, J. N. Becker, C. Weinzetl, I. A. Walmsley, and P. M. Ledingham, "Gigahertz-bandwidth optical memory in Pr^{3+}:Y_2SiO_5," Opt. Lett. **46**(12), 2948–2951 (2021).
24. F. K. Asadi, J. -W. Ji, and C. Simon, "Proposal for transduction between microwave and optical photons using ^{167}Er -doped yttrium orthosilicate," Phys. Rev. A **105**(6), 062608 (2022).
25. M. Afzelius, I. Usmani, A. Amari, B. Lauritzen, A. Walther, C. Simon, N. Sangouard, J. Minář, H. de Riedmatten, N. Gisin, and S. Kröll, "Demonstration of atomic frequency comb memory for light with spin-wave storage," Phys. Rev. Lett. **104**(4), 040503 (2010).
26. T. Chanelière, J. Ruggiero, M. Bonarota, M. Afzelius, and J. Le Gouët, "Efficient light storage in a crystal using an atomic frequency comb," New J. Phys. **12**(2), 023025 (2010).
27. H. de Riedmatten, M. Afzelius, M. U. Staudt, C. Simon, and N. Gisin, "A solid-state light-matter interface at the single-photon level," Nature **456**(7223), 773–777 (2008).
28. M. Bonarota, J. Ruggiero, J. Le Gouët, and T. Chanelière, "Efficiency optimization for atomic frequency comb storage," Phys. Rev. A **81**(3), 033803 (2010).
29. P. Jobez, N. Timoney, C. Laplane, J. Etesse, A. Ferrier, P. Goldner, N. Gisin, and M. Afzelius, "Toward highly multimode optical quantum memory for quantum repeaters," Phys. Rev. A **93**(3), 032327 (2016).
30. S. Yasui, M. Hiraishi, A. Ishizawa, H. Omi, R. Kaji, S. Adachi, and T. Tawara, "Precise spectroscopy of ^{167}Er:Y_2SiO_5 based on laser frequency stabilization using a fiber laser comb," Opt. Express **29**(17), 27137–27148 (2021).
31. T. Tawara, G. Mariani, K. Shimizu, H. Omi, S. Adachi, and H. Gotoh, "Effect of isotopic purification on spectral-hole narrowing in $^{167}Er^{3+}$ hyperfine transitions," Appl. Phys. Express **10**(4), 042801 (2017).
32. H. Vries and D. A. Wiersma, "Photophysical and photochemical molecular hole burning theory," J. Chem. Phys. **72**(3), 1851–1863 (1980).
33. E. S. Maniloff, F. R. Graf, H. Gygax, S. B. Altner, S. Bernet, A. Renn, and U. P. Wild, "Power broadening of the spectral hole width in an optically thick sample," Chem. Phys. **193**(1-2), 173–180 (1995).
34. T. Böttger, Y. Sun, C. W. Thiel, and R. L. Cone, "Spectroscopy and dynamics of Er^{3+}:Y_2SiO_5 at 1.5 μm," Phys. Rev. A **74**(7), 075107 (2006).
35. E. Z. Cruzeiro, A Tiranov, J. Lavoie, A. Ferrier, P. Goldner, N. Gisin, and M. Afzelius, "Efficient optical pumping using hyperfine levels in $^{145}Nd^{3+}$:Y_2SiO_5 and its application to optical storage," New J. Phys. **20**(5), 053013 (2018).
36. G. H. Larson and C. D. Jeffries, "Spin-lattice relaxation in some rare-earth salts. II. angular dependence, hyperfine effects, and cross relaxation," Phys. Rev. **145**(1), 311–324 (1966).
37. S. R. Hastings-Simon, B. Lauritzen, M. U. Staudt, J. L. M. van Mechelen, C. Simon, H. de Riedmatten, M. Afzelius, and N. Gisin, "Zeeman-level lifetime in Er^{3+}:Y_2SiO_5," Phys. Rev. B **78**(8), 085410 (2008).
38. E. Baldit, K. Bencheikh, P. Monnier, S. Briaudeau, J. A. Levenson, V. Crozatier, I. Lorgeré, F. Bretenaker, J. L. Le Gouët, O. Guillot-Noël, and Ph. Goldner, "Identification of Λ-like systems in Er^{3+}:Y_2SiO_5 and observation of electromagnetically induced transparency," Phys. Rev. B **81**(14), 144303 (2010).
39. B. Lauritzen, S. R. Hastings-Simon, H. de Riedmatten, M. Afzerius, and N. Gisin, "State preparation by optical pumping in erbium-doped solids using stimulated emission and spin mixing," Phys. Rev. A **78**(4), 043402 (2008).
40. M Afzelius and C. Simon, "Impedance-matched cavity quantum memory," Phys. Rev. A **82**(2), 022310 (2010).

OPTICS CONTINUUM

41. M. Sabooni, Q. Li, S. Kröll, and L. Rippe, "Efficient quantum memory using a weakly absorbing sample," Phys. Rev. Lett. **110**(13), 133604 (2013).
42. D. -C. Liu, P. -Y. Li, T. -X. Zhu, L. Zheng, J. -Y. Huang, Z. -Q. Zhou, C. -F. Li, and G. -C. Guo, "On-demand storage of photonic qubits at telecom wavelengths," arXiv:2201.03692 (2022).
43. M. Gündoğan, M. Mazzera, P. M. Ledingham, M. Cristiani, and H. de Riedmatten, "Coherent storage of temporally multimode light using a spin-wave atomic frequency comb memory," New J. Phys. **15**(4), 045012 (2013).